Energy-Management Method to Reduce the Capacity of Lithium-Ion Batteries in Hybrid-Voltage-Source Three-Level Inverter for DC-Electrified Railway Vehicles

TADASHI MIZOBUCHI [1], **KEIICHIRO KONDO**[2] **(Member, IEEE), YOSUKE DAIRAKU** [3,4],
TAKESHI SHINOMIYA[4], **AND KATSUMI ISHIKAWA**[4]

[1]School of Advanced Science Engineering, Waseda University, Tokyo 169-8050, Japan
[2]Faculty of Science Engineering, Waseda University, Tokyo 169-8050, Japan
[3]Chiba University, Chiba 263-8522, Japan
[4]Railway Systems Business Unit, Hitachi Ltd., Ibaraki 317-0056, Japan

CORRESPONDING AUTHOR: TADASHI MIZOBUCHI (e-mail: tmizobuchi@toki.waseda.jp)

ABSTRACT The hybrid-voltage-source three-level inverter is a traction circuit system aimed at realizing energy savings with lithium-ion batteries for direct-current-electrified railway vehicles. However, this system has the limitation of being unable to freely control the power flow of the batteries owing to the pulse width modulation. However, because this system has batteries, energy management is required for the batteries. Therefore, it is necessary to propose an energy-management method that achieves the required energy-saving effect while considering the constraints of the battery power control. In this paper, a management method is proposed to control the power flow of the batteries by determining the pulse mode of the inverter and the modulation wave offset based on the state of the charge and inverter frequency. In a 0.75-kW class mini-model verification, the effectiveness of the proposed energy-management method is then confirmed based on the state of the charge, inverter frequency, offset, and battery power. Subsequently, we evaluate the energy-saving effect of this hybrid system using a numerical simulation while considering an actual railway vehicle. In addition, the optimal capacity of the batteries is investigated. As a result, the best energy-saving effect is obtained when two of the assumed batteries are connected in series and three in parallel, and the power consumption is reduced by approximately 21%.

INDEX TERMS Battery management systems, energy management, hybrid power systems, induction motors, inverters, lithium batteries.

I. INTRODUCTION

One of the methods for achieving energy savings in railway vehicle traction is to improve the motor torque characteristics by boosting the inverter output voltage, thereby improving acceleration performance during powering and reducing the consumption energy by increasing the regenerative energy during deceleration. In particular, various types of traction circuit systems that use energy storage devices to boost the inverter output voltage have been developed in recent years. One of them is a system in which energy storage devices are connected in series with an overhead line power source through a converter [1]. Other systems that boost the voltage by connecting energy storage devices and a direct-current/direct-current (DC/DC) converter in parallel to the overhead line power source have also been investigated [2]–[4]. In these systems, although there is a difference in the circuit configuration method of the energy storage devices, all these systems aim to improve the output power by boosting the inverter input voltage, i.e., filter capacitor voltage. In contrast, the hybrid-voltage-source three-level inverter (hybrid 3Lv. VSI) is an application of multilevel converters, which are usually applied to drive systems and power systems that require a
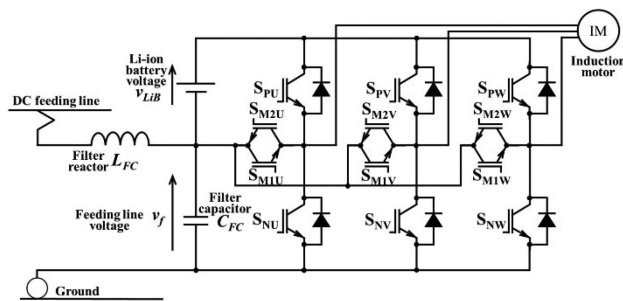
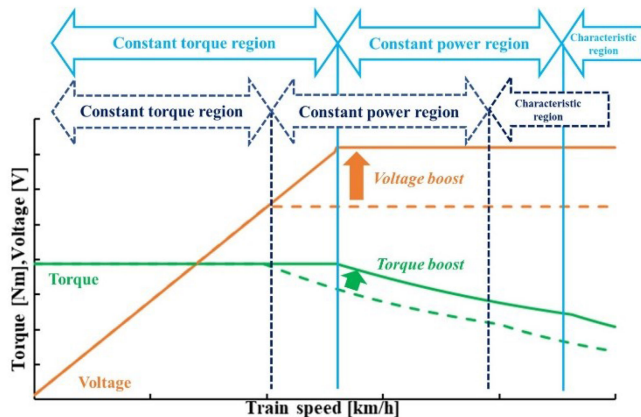**FIGURE 1.** Hybrid voltage source three level inverter.

FIGURE 2. Improved motor characteristics.

high anti-voltage capacity [5]–[7]. As shown in the circuit diagram in Fig. 1, a three-level inverter is applied, and one of the two voltage sources is assigned to the overhead line source and the other to the energy storage devices [8]. In this system, lithium-ion batteries (LiBs) are used as energy storage devices. Therefore, the inverter output voltage is boosted, and the constant torque region is expanded by the value of the battery voltage. The energy capacity of the LiBs can be reduced because they only assist the additional voltage.

The hybrid 3Lv. VSI is operated under pulse width modulation (PWM) with two carrier waves and one modulation wave to combine the overhead line power and storage devices' power for providing the alternating current (AC) side, and the gate signal of the switching devices and output voltage are determined [9], which is in contrast to the multilevel inverter system comprising the use of single carrier waves [10], [11], which is aimed at bidirectional power flow. Because two modulation waves are used, one for each power source, it is possible to control the power distribution between the two voltage sources by changing the output voltage. In contrast, in the hybrid 3Lv. VSI, the power flow of the batteries is limited by the inverter output voltage. Furthermore, the energy management of the batteries is essential for maintaining the battery energy within the limits to prevent under voltage or overvoltage and extend battery life [12]. Therefore, it is necessary to propose an energy management method that can maintain the energy-saving effect under the restriction of the power distribution

at a certain output voltage. Furthermore, the optimal battery capacity based on the proposed energy-management method must be studied for practical applications.

The remainder of this paper is organized as follows. First, the energy-management method for the battery of the hybrid 3Lv. VSI is proposed. Then, scaled-down mini-model experiments are conducted to verify the effectiveness and operability of the proposed power flow control method. Finally, the energy-saving effect and optimal battery capacity are verified using a numerical simulation wherein actual railway vehicles are considered.

II. HYBRID-VOLTAGE-SOURCE THREE-LEVEL INVERTER
A. ENERGY-SAVING EFFECT WITH IMPROVED MOTOR CHARACTERISTICS

Fig. 2 presents the characteristics of the induction motor (IM) torque and applied voltage versus train speed. The total speed range can be divided into three ranges based on the distinctive features of these characteristics. The first range comprises the constant-torque region. In this region, the output voltage slope (the value of voltage/frequency) is maintained constant, and the motor can output the maximum torque. The next range comprises the constant-power region or the characteristic region, wherein the motor is operated under a weakening flux control with a constant voltage. Therefore, the motor torque is inversely proportional to the train speed, as shown in Fig. 2.

The range of the constant-torque region is determined by the maximum inverter output voltage. Therefore, on boosting the output voltage, this region is expanded, and the constant power and motor characteristics regions are shifted to a higher speed range. This improves the torque characteristics in the medium-to-high-speed range.

By improving the torque characteristics, two energy-saving effects are realized. The first effect is the shortening of the powering time by improving the acceleration performance. The second effect is an increase in regenerative energy by improving the torque characteristics.

Thus, it is possible to obtain energy-saving effects by boosting the output voltage of the inverter.

B. CIRCUIT CONFIGURATION

Fig. 1 presents the system and circuit configuration of the hybrid 3Lv. VSI that is aimed at boosting the inverter output voltage. Each motor car has a traction circuit system. The system configuration is the same as that of a normal two-level inverter system, except that the inverter is connected to the overhead line side with a filter reactor and filter capacitor. The induction motor is connected to the inverter output side, and four motors are driven simultaneously by one inverter.

The inverter circuit configuration is based on the application of a T-type neutral-point-clamped 3Lv. inverter [13], [14]. As the semiconductor devices are in the middle arm ($S_{M1X(X=U,V,W)}$, S_{M2X}), it is assumed that reverse blocking insulated-gate bipolar transistors are used. For the other arms, the normal IGBTs are used as switching devices (S_{PX}, S_{NX}).
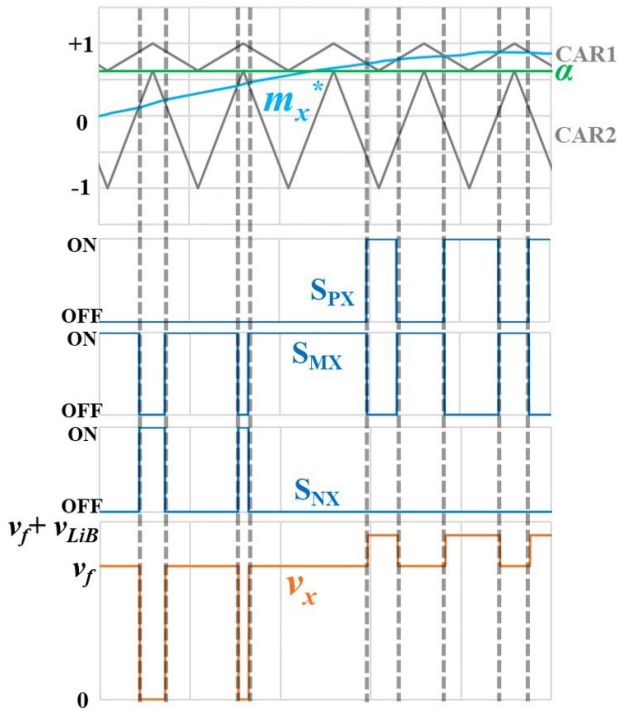
FIGURE 3. PWM pulse generation in hybrid 3Lv. VSI.

FIGURE 4. Power flow control by the modulation wave offset.

Another feature of this circuit system is that two different DC voltage sources are used. The overhead line voltage is defined as v_f, and the voltage of the LiBs is defined as v_{LiB}.

C. PWM SWITCHING MODE

The PWM switching pattern is determined as shown in Fig. 3. It is operated using asynchronous PWM—as in a normal two-level inverter—but the hybrid 3Lv. VSI uses two carrier waves to generate pulses [15]. The ratio of the amplitudes of each carrier wave is equal to the voltage of the two voltage sources. In Fig. 3, the carrier wave on the LiBs side is denoted as CAR1, and that on the overhead line side is denoted as CAR2. The modulation wave is defined as m_x^*. The maximum value of CAR1 is $+1$, and the minimum value of CAR2 is -1. The boundary line of each carrier α is defined as follows.

$$\alpha = \frac{v_f - v_{LiB}}{v_f + v_{LiB}} \tag{1}$$

In addition, the logic of the PWM is as follows.

If $m_x^* >$ CAR1, $S_{PX(X=U,V,W)}$ is on.
If CAR1 $> m_x^* >$ CAR2, S_{M1X} or S_{M2X} is on. (2)
If $m_x^* <$ CAR2, S_{NX} is on.

When the upper device S_{PX} is on, the output voltage is $v_f + v_{LiB}$. As described above, the output voltage of the hybrid 3Lv. VSI is determined. However, it is impossible to control the charging or discharging power of LiBs using only the PWM method. This is because the two voltage sources
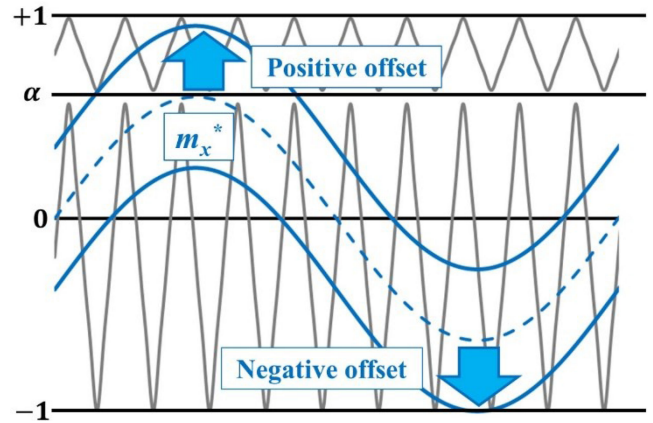
output a single AC voltage waveform instead of applying the sum of the AC voltage from each voltage source to the AC side. To make it possible to manage the charging or discharging of LiBs within this constraint, power flow control is used with a modulation wave offset between each voltage source. By adding an offset to the modulation wave, the positional relationship between the two carrier waves and modulation wave is changed. This facilitates the power flow control of the two voltage sources. Fig. 4 presents a schematic of the power-flow control. The addition of a positive offset causes the modulation wave to move to the LiBs' carrier wave side. The negative offset changes the modulation wave such that it crosses the carrier wave of the overhead line. These offsets must be zero in the high-speed region, where the amplitude of the modulation wave is greater than 1.

III. ENERGY-MANAGEMENT METHOD OF HYBRID 3LV. VSI

A. BASIC ENERGY MANAGEMENT

In this hybrid system comprising the use of LiBs, a charge/discharge management method for LiBs is also necessary. Specifically, the management method prevents the over-charging and over-discharging of the batteries. In the case of other hybrid systems, an energy-management method to manage the state of the charge (SOC) of the batteries while controlling the output power of each power source has been proposed [16]. Alternatively, in this system, the power of each voltage source cannot be controlled freely owing to the constraints imposed by the PWM operation. Because there is a close relationship between the power flow control and PWM, an energy-management method is required to determine the pulse mode and the offset according to the amplitude of the modulation wave while managing the SOC of LiBs. Therefore, we propose an energy-management method based on two variables: the inverter frequency and SOC. In addition, the pulse mode and offset in the proposed management method should be determined such that the energy-saving effect can be realized.
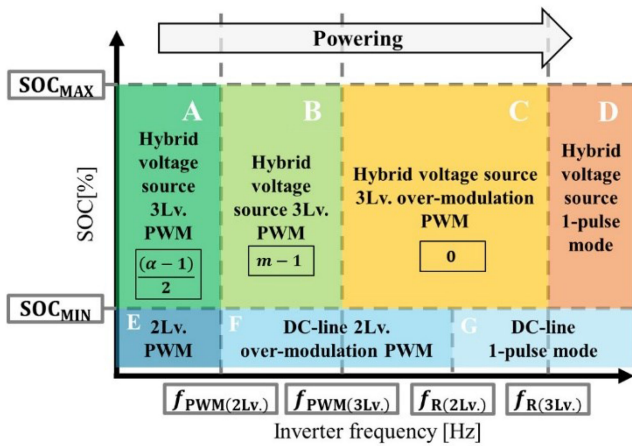
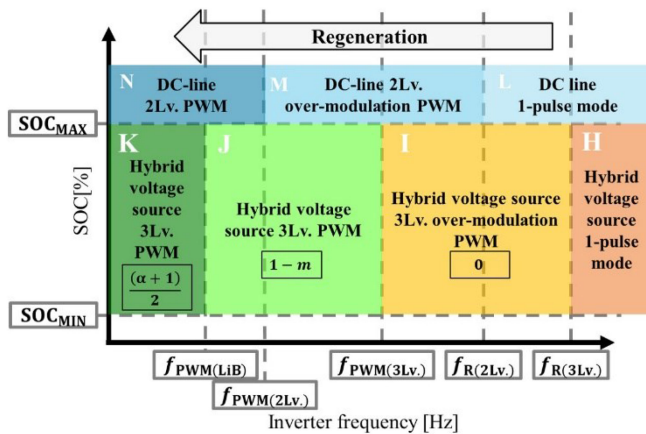**FIGURE 5.** Selection of offset and pulse mode in powering.

FIGURE 6. Selection of offset and pulse mode in regeneration.

Furthermore, a limitation is implemented in the offset to reduce the harmonic current of the batteries [17]. The energy-management method that takes into consideration these conditions is presented in Figs. 5–6. The management methods used for powering and regeneration are explained separately.

B. ENERGY MANAGEMENT FOR POWERING

An energy-management method for powering is proposed, as shown in Fig. 5. The PWM examples for each output voltage are listed in Table 1. The alphabets in Fig. 5 correspond to those in and Table 1.

Along the vertical axis in Fig. 5, the maximum and minimum SOC for preventing over-charging and over-discharging are defined as SOC_{MAX} and SOC_{MIN}, respectively. Because the batteries only discharge during powering, the system operates in the non-boosting two-level PWM mode by the overhead DC-line voltage and does not discharge from the LiBs when the SOC is less than SOC_{MIN} in all the speed bands. When $SOC_{MIN} < SOC < SOC_{MAX}$, the system operates in the hybrid voltage source three-level PWM mode. The horizontal axis indicates the inverter frequency, and the right side

of the figure presents a higher train speed. Because the pulse mode is also switched depending on the inverter frequency, the boundary frequencies are defined as f_{PWM} and f_R, where f_{PWM} is the terminal frequency of each PWM region, and f_R is the rated frequency or the terminal of the constant torque region. Because there are four pulse-mode regions for the frequencies along the horizontal axis.

Table 1 summarizes the possible values of the output voltage, offset, and LiBs discharging state when the map is divided into the areas A–G. In area A, the center of the modulation wave is shifted to that of the lower (overhead line voltage) carrier wave by adding an offset. Because the amplitude of the modulation wave does not exceed that of the lower carrier, the modulation wave does not intersect the upper carrier wave, and the LiBs do not discharge. In area B, because the modulation wave amplitude is greater than the lower carrier, the center of the modulation wave gradually approaches zero as the modulation wave becomes larger. In area B, the LiBs start discharging. In area C, the modulation rate is greater than 1, and the inverter is operated with over-modulation PWM, and no offset is added. In area D, it is operated in hybrid voltage source 1-pulse mode with a constant output voltage. In areas E, F, and G below SOC_{MIN} in Fig. 5, it is operated with PWM, over-modulation PWM, and 1-pulse mode by overhead DC-line power source. The inverter output voltage is not boosted, and the LiBs do not discharge at all.

C. ENERGY MANAGEMENT FOR REGENERATION

We propose an energy-management method for regeneration, as shown in Fig. 6. The PWM examples in each area are listed in Table 2. The alphabets in Fig. 6 correspond to those in Table 2.

The vertical and horizontal axes in the map denote the SOC and inverter frequency, as in the case of powering. The inverter frequency $f_{PWM(LiB)}$ is defined as the frequency at which the amplitude of the upper carrier wave is equal to that of the modulation wave. The maximum and minimum values of the SOC are the same as those in the powering map. During regeneration, when the SOC is greater than SOC_{MAX}, the inverter operates in the overhead-line-voltage two-level PWM mode and does not charge the LiBs. The design guideline for the hybrid voltage source three-level PWM mode of the energy management during regeneration is proposed to charge the LiBs in all the speed regions. By continuing to charge the LiBs to the maximum energy during regeneration, the system starts at the highest possible SOC during the next powering operation.

The map is divided into the areas H–M, and the possible output voltage, offset value, and LiBs charging state are summarized in Table 2. Area H indicates the hybrid voltage source 1-pulse mode. Area I indicates the hybrid voltage source three-level over-modulation PWM mode, and no offset is added to the modulation wave. In area J, the amplitude of the modulation wave is greater than that of the upper carrier wave, and a positive offset is added as the inverter frequency decreases. In area K, the modulation wave amplitude is less
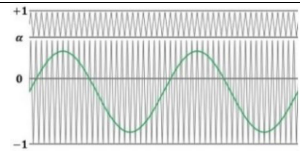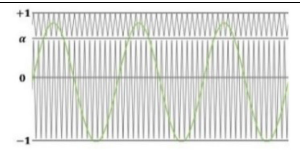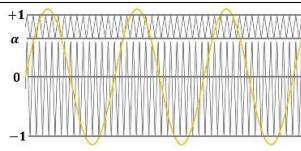
TABLE 1 PWM Examples and Each Variable in Powering

Area	A	B	C	D
Pulse mode	Hybrid voltage source 3Lv. PWM	Hybrid voltage source 3Lv. PWM	Hybrid voltage source 3Lv. over-modulation PWM	Hybrid voltage source 1-pulse
Output voltage [V]	$0 - \dfrac{\sqrt{6}}{4} v_f$	$\dfrac{\sqrt{6}}{4} v_f - \dfrac{\sqrt{6}}{4}\left(v_f + v_{LiB}\right)$	$\dfrac{\sqrt{6}}{4}\left(v_f + v_{LiB}\right) - \dfrac{\sqrt{6}}{\pi}\left(v_f + v_{LiB}\right)$	$\dfrac{\sqrt{6}}{\pi}\left(v_f + v_{LiB}\right)$
Offset value	$\dfrac{(\alpha - 1)}{2}$	$m - 1 \quad \therefore \dfrac{(\alpha - 1)}{2} - 0$	0	0
PWM modulation wave				-
Discharging status of LiBs	×	○	○	○

TABLE 2 PWM Examples and Each Variable in Regeneration
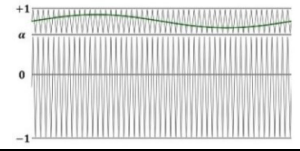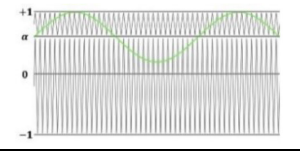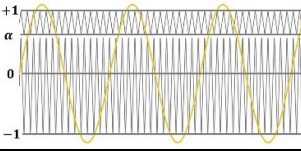
Area	K	J	I	H
Pulse mode	Hybrid voltage source 3Lv. PWM	Hybrid voltage source 3Lv. PWM	Hybrid voltage source 3Lv. over-modulation PWM	Hybrid voltage source 1-pulse
Output voltage [V]	$0 - \dfrac{\sqrt{6}}{4} v_{LiB}$	$\dfrac{\sqrt{6}}{4} v_{LiB} - \dfrac{\sqrt{6}}{4}\left(v_f + v_{LiB}\right)$	$\dfrac{\sqrt{6}}{4}\left(v_f + v_{LiB}\right) - \dfrac{\sqrt{6}}{\pi}\left(v_f + v_{LiB}\right)$	$\dfrac{\sqrt{6}}{\pi}\left(v_f + v_{LiB}\right)$
Offset value	$\dfrac{(\alpha + 1)}{2}$	$1 - m \quad \therefore \dfrac{(\alpha + 1)}{2} - 0$	0	0
PWM modulation wave				-
Charging status of LiBs	○	○	○	○

TABLE 3 Induction Motor Data

Parameters	Symbols	Value
Poles	–	4
Rated power	P	0.75 kW
Rated voltage	V	200 V
Rated current	I	3.8 A
Rated frequency	F	50 Hz
Stator resistance	R_1	4.0 Ω
Rotor resistance	R_2	2.2 Ω
Stator inductance	L_1	0.173 H
Rotor inductance	L_2	0.175 H
Mutual inductance	M_m	0.163 H

than that of the upper carrier wave. An offset is then added to align the center of the modulation wave with that of the upper carrier wave. Therefore, the LiBs are charged in all areas, i.e., from area H to K. Areas L to M are operated in the overhead-line two-level mode for all the speed ranges. Because the LiBs are not charged, the SOC does not increase beyond SOC_{MAX}.

IV. EXPERIMENTAL VERIFICATION OF PROPOSED METHOD USING MINI-MODEL SYSTEM

A. OUTLINE OF EXPERIMENTS

In Section III, the energy management method for the hybrid 3Lv. VSI is proposed. In the proposed management method, the pulse mode of the inverter and the offset are selected according to the inverter frequency and SOC of the LiBs, and it is necessary to verify that they are selected correctly. To verify the effectiveness of the management method, a 0.75-kW-class induction-motor experimental system with an inertial load is used, as shown in Figs. 7–9; the batteries are evaluated using a regenerative DC source whose voltage varied with SOC and its current. For the experiment, four run patterns with different SOC variations are prepared. In each run pattern with a different SOC variation, we check whether the pulse mode and offset are correctly selected based on the
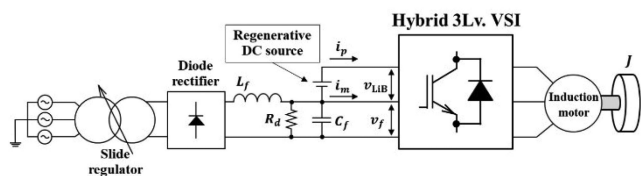
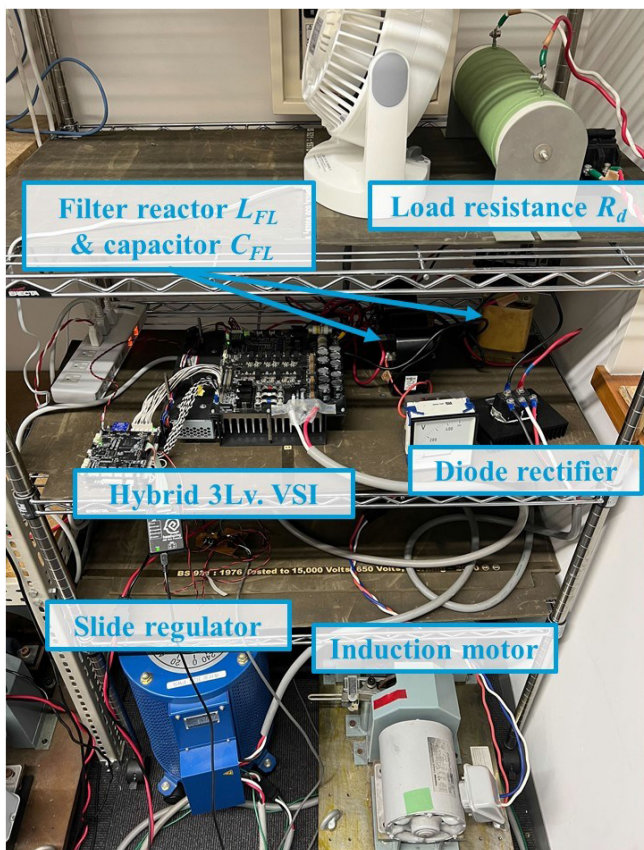**FIGURE 7.** Mini-model experimental system.

FIGURE 8. Mini-model experimental system appearance.

SOC and inverter frequency simultaneously. We also verify that the LiBs charging/discharging power flow is controlled by the selected pulse mode and offset. Therefore, the inverter output voltage, offset, and LiBs' power and LiBs' energy in each of these running patterns are measured via experimental tests.

B. EXPERIMENTAL CONDITIONS

The parameters of the experimental system are listed in Tables 3–4. The mini-model experimental system is used to verify the power flow control performance of the PWM in the proposed hybrid 3Lv. VSI configurations. Therefore, the mini-model experimental system can be verified that the proposed energy management method determines the pulse mode and modulated wave offset only by SOC and inverter frequency, though the experimental system is different scale ratio among voltage, current, power and energy from those used in the traction
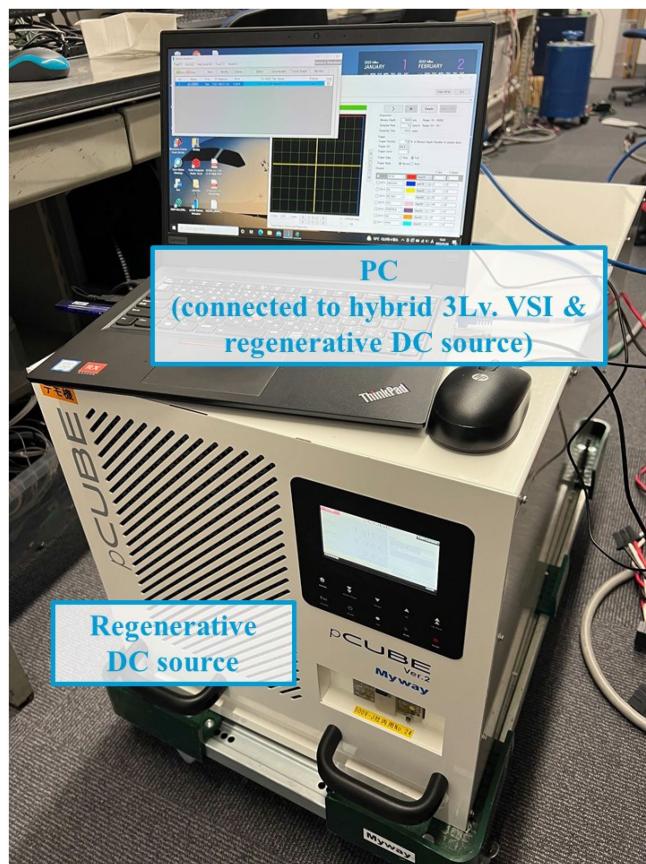

FIGURE 9. Regenerative DC source appearance.

TABLE 4 Circuit Parameters

Parameters	*Symbols*	*Value*
Load resistance	R_d	100 Ω
Filter reactor	L_f	0.5 mH
Filter capacitor	C_f	800 μF
Flywheel inertia	J	0.48 kg·m^2
Line voltage	v_f	200 V

electric components system of a real railway vehicle. The constants used in the control are listed in Table 5. In a mini-model experimental system, a DC regenerative power supply is used as a substitute power supply for the LiBs. Thus, the SOC of the power supply cannot be determined. Therefore, a virtual SOC is calculated by setting the charge and discharge energy and virtual capacity of the DC regenerative power supply and is used for the energy management. In addition, the voltage of the DC regenerative power supply does not fluctuate according to the emulated SOC. The emulated SOC, i.e., SOC$_{emu}$, is calculated using equation (3).

$$\text{SOC}_{emu} = \frac{(E_{initial} - E_{LiB})}{E_{capacity}} \times 100 [\%] \qquad (3)$$

TABLE 5 Control Parameters

Parameters	Symbols	Value
Control cycle	-	200 μs
PWM carrier frequency	f_c	5 kHz
Dead time	T_{dead}	3 μs
Automatic current control time constant	τ_{ACR}	10 ms
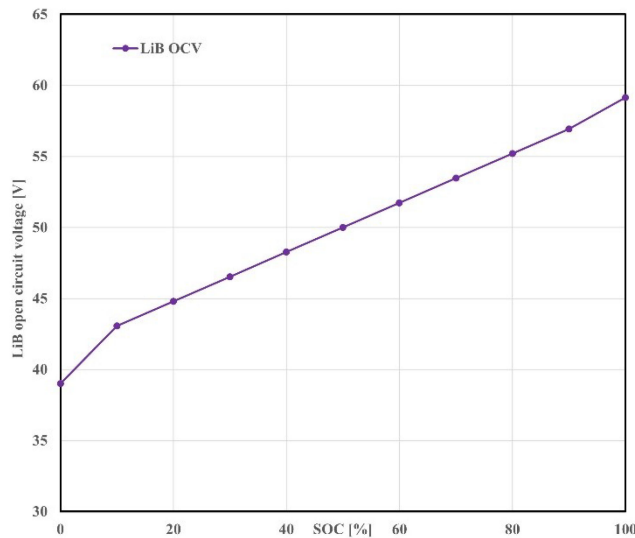
FIGURE 10. Open-Circuit-Voltage characteristics in regenerative DC source.

FIGURE 11. Current-voltage characteristics in regenerative DC source.

TABLE 6 Run Patterns

Run Pattern	$E_{initial}$ [Wh]	$E_{capacity}$ [Wh]	SOC_{MIN} [%]	SOC_{MAX} [%]
#1	0.96			
#2	0.6	1.2	20.0	80.0
#3	0.24			
#4				50.0

$E_{initial}$ is the assumed initial energy of the regenerative DC power supply that emulates the batteries, and E_{LiB} is its input or output energy. $E_{capacity}$ is the assumed energy capacity of the virtual LiBs. In this experiment, E_{LiB} is a measurable value, and the emulated SOC can be calculated by setting the values of $E_{initial}$ and $E_{capacity}$. The offset and pulse modes are selected according to the emulated SOC and the inverter frequency, as described above.

To simulate the LiBs characteristics with regenerative DC source, the open-circuit-voltage (OCV) is changed with SOC_{emu} and the current [18]–[20]. The emulated OCV characteristic for the experiments is presented in Fig. 10. When the SOC decreases, the OCV decreases similarly. In Fig. 10, when SOC is between 10% and 90%, the rate of change of OCV is constant. However, when the SOC is below 10% or above 90%, the rate of change of OCV increases compared to the rate of change of 10% to 90%. In addition, there is DCIR (Direct Current Internal Resistance) in the LiB, and the output voltage changes depending on the current. Therefore, the current-voltage characteristics are presented in Fig. 11. The DCIR is equal to the slope of the current-voltage characteristic, and is set to 1.0Ω.

To conduct experiments with run patterns with four different SOC variations, as shown in Table 6, multiple run patterns are prepared, wherein $E_{initial}$ and SOC_{MIN} are varied. Table 6 lists the $E_{initial}$ and SOC_{MIN} for each run pattern. The range of
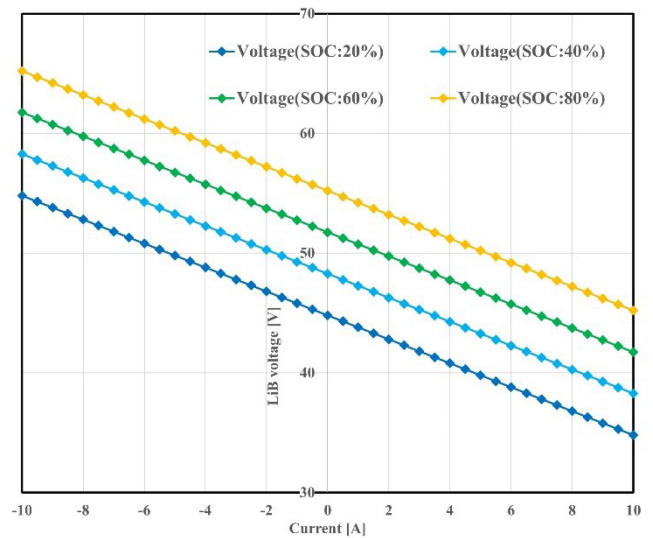
SOC in the energy management method is set to 20% to 80%, emulating the actual LiB's operation range in which its life-long is considered. In the case of #1, because the initial SOC is sufficiently high, hybrid 3Lv. VSI operates in the three-level PWM mode for both powering and regeneration. In the case of #2, because the initial SOC is relatively low, it shifts to the two-level PWM mode from the three-level PWM mode during powering and operates in the three-level PWM mode during regeneration. In case #3, the SOC reaches SOC_{MIN} in the beginning, which means that the LiBs are not discharged. Therefore, the inverter operates in the non-boost mode during powering, but in the boost mode during regeneration. In the case of #4, in contrast to #3, hybrid 3Lv. VSI switches to a two-level PWM mode in the middle of the regeneration. From this, it is assumed that the LiBs are sufficient charged during the regeneration.

The dq-axis current command values are given to output a constant torque at the rated frequency. The weakening flux control is operated in the region wherein the output voltage becomes constant. During regeneration, the motor is operated in the constant-torque region for all the speed ranges. In any running pattern, the motor accelerates until the rotor frequency reaches 60.0 Hz, and when it reaches 59.8 Hz after coasting, it starts a regenerative operation until it reaches 0 Hz.
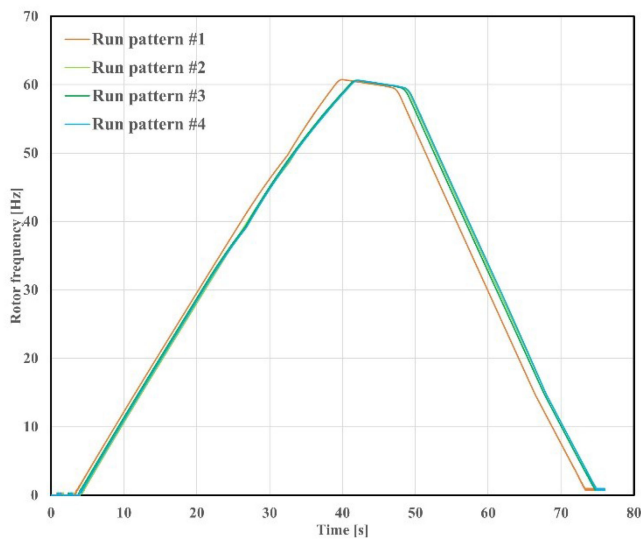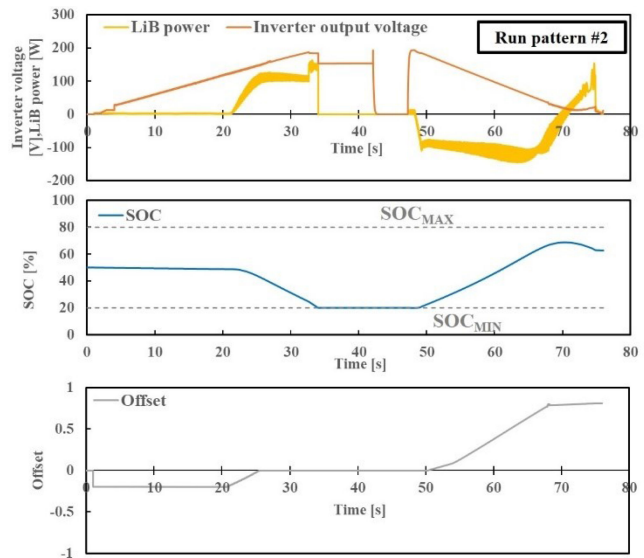
FIGURE 12. Rotor frequency.
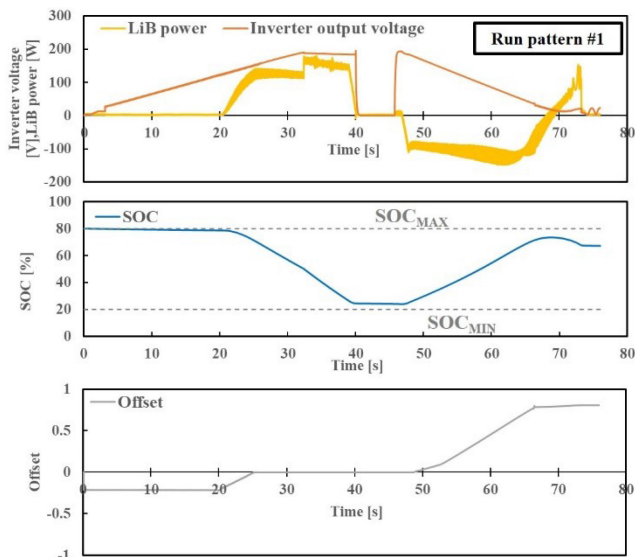

FIGURE 14. Results of run pattern #2.

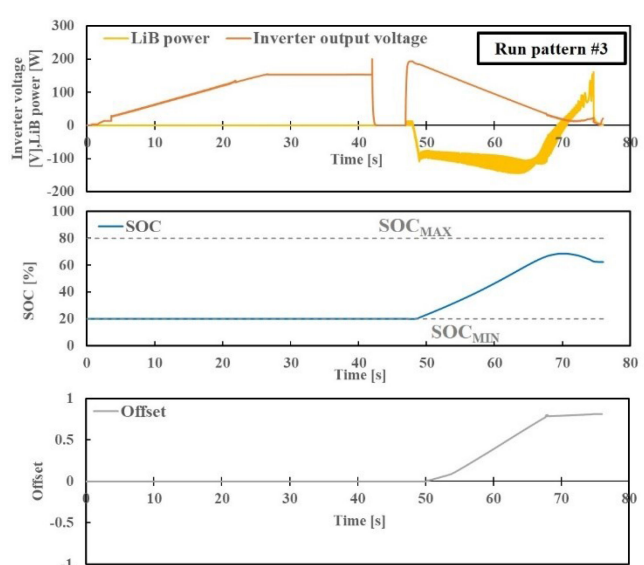**FIGURE 13. Results of run pattern #1.**

FIGURE 15. Results of run pattern #3.

C. EXPERIMENTAL RESULTS
1) RUN CURVE OF EACH RUNNING PATTERN
The rotor frequency curves are presented in Fig. 12. Figs. 13 –16 present the inverter output voltage, SOC, offset, and LiB power for each run pattern.

From Fig. 12 and the inverter output voltage in Fig. 13, run pattern #1 is operated in the hybrid voltage source mode during powering and exhibits a high acceleration performance and the fastest time to reach the maximum speed. In the case of #2, as shown in Fig. 13, the inverter output voltage switches to the two-level mode at approximately 32 s, and the acceleration performance is slightly lower than that in the case of #1. Although there is a difference in the pulse mode during regeneration for #3 and #4, there is no difference in the deceleration in the results of Fig. 12. This is because the time

for switching to the DC-line two-level mode in #4 is within the constant-torque region.

3) OFFSET AND LIB POWER
As shown in Fig. 13, we focus on the relationship between the offset and the power of the LiBs for run pattern #1 to confirm that the power flow control of the LiBs is achieved. When the offset is -0.2 after the start of powering, the value of the SOC is within the limits of SOC_{MAX} and SOC_{MIN} in Fig. 5, and the inverter frequency is between 0 and $f_{PWM(2Lv.)}$, depending on the value of the output voltage. Therefore, this section is in area A. In area A, according to Table 1, the offset value is -0.2 because α is 0.6 from equation (1) in this experiment. Thus, the LiBs do not discharge, and the power of the LiBs is zero in the experimental results as well.
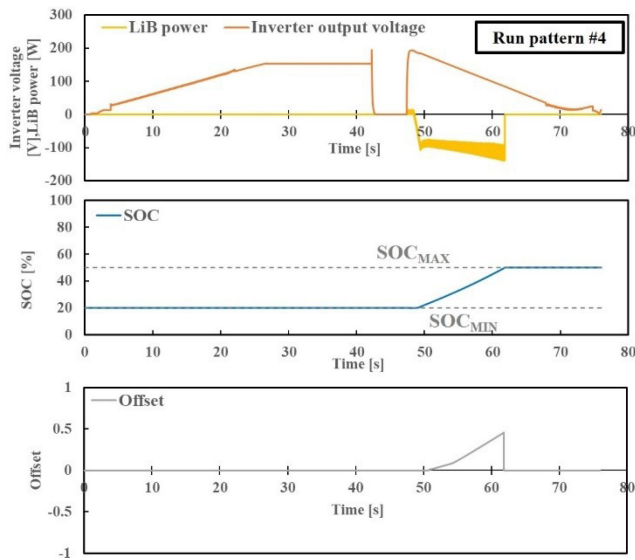
FIGURE 16. Results of run pattern #4.

After this, the offset gradually changes from −0.2 to 0. Because the offset corresponds to the section with $m - 1$, this section is regarded as area B. In the high-speed region after area B, the offset is maintained at 0 in boost-mode powering; this is indicated by areas C and D in Fig. 5. In these areas, the LiB power exhibits a positive value, which indicates that the LiBs are discharging.

During regeneration, the SOC is consistently within the limit, and the inverter operates in the hybrid voltage source three-level PWM mode. At approximately 49 s, the offset is 0, which is indicated by area I. The output voltage is then within the range of area I, as shown in Table 2. Subsequently, the offset continues to increase until the output voltage reaches 30 V. This section corresponds to area J, and the offset and output voltage values in Table 2 are obtained as the experimental results. The lower speed range comprises area K, and the offset is maintained at 0.8, as α is 0.6.

This offset change facilitates a charging operation in all the speed regions during regeneration, as shown in Table 2, and the LiB power exhibits a negative value; thus, it is confirmed that the LiBs are charging. However, it is confirmed that the LiB power switches to a positive value at 68 s; thus, the LiBs are discharging. This is considered to indicate that the discharging is caused by resistance of the filter reactor and not by the power flow control with the offset.

Therefore, the modulation wave offset is selected as listed in Tables 1 and 2, according to the inverter frequency, i.e., the output voltage at that time. Furthermore, the offset facilitates the power flow control of the LiB charging or discharging. In addition, the power flow control of the LiB is not prevented by the effect of the voltage changes due to the LiB's SOC.

It is shown in Section II that the PWM control of the hybrid 3Lv. VSI inhibits the precise control of the LiBs' power. This is demonstrated by the fact that the power value cannot be controlled to a certain value in the mini-model experiment.

3) SELECTION OF PULSE MODE BASED ON SOC

In this section, we focus on the selection of the pulse mode based on the SOC in each run pattern. In the case of run pattern #1, hybrid 3Lv. VSI is constantly operated in hybrid voltage source three-level PWM or 1-pulse mode because the SOC is within the limits. Therefore, the LiBs discharge during powering and charge during regeneration.

In the case of run pattern #2, the offset value is selected correctly in the hybrid voltage source three-level PWM mode, as in #1. However, the SOC reaches SOC_{MIN} at 33 s, as shown in Fig. 14, and it is necessary to switch to the non-boost mode. The output voltage changes from 195 V to 155 V, which means that the maximum voltage value in the hybrid voltage source 1-pulse mode changes to that in the overhead DC-line 1-pulse mode.

The run pattern #3 is used for the case wherein the SOC is SOC_{MIN} at the start of powering. The offset is maintained at 0 during powering, and the output voltage indicates that the inverter operates in the non-boost mode. Thus, the LiBs do not discharge during powering. In the case of run patterns #2 and #3, during regeneration, the SOC is less than SOC_{MAX}, and the inverter is operated in the hybrid voltage source three-level PWM mode.

In the case of run pattern #4, the SOC reaches SOC_{MAX} in the middle of regeneration and switches to the overhead DC-line two-level PWM mode. The SOC reaches SOC_{MAX} at approximately 62 s, and the offset changes to 0. There is no change in the output voltage because the inverter is operated in the constant-torque region. However, as the LiBs' power becomes 0, switching to a two-level PWM mode is achieved at that time.

From these results, it is verified that the pulse mode is selected according to the SOC value. Finally, from the relationships of the offset and LiBs' power, and pulse mode, we confirm that the charging or discharging power flow of the LiBs is controlled by the selected pulse mode and offset based on proposed energy-management method.

V. REDUCTION OF ENERGY CONSUMPTION AND OPTIMIZING LIB CAPACITY VIA NUMERICAL SIMULATION
A. OUTLINE OF SIMULATION

In Sections III and IV, the energy-management method for hybrid 3Lv. VSI is proposed. In the proposed method, the pulse mode is determined according to the inverter frequency and SOC of the LiBs, which also determines the operation methods of this circuit system. Therefore, it is necessary to confirm the extent of the energy saving effect achieved in this circuit, of which the operation method has been decided. It is also necessary to select the optimal LiB capacity for practical application. Generally, an increase in the number of LiBs is considered to extend the time required for boosting the output voltage, but optimizing the LiBs' capacity is necessary to extract the maximum energy saving effect from the viewpoint of on-board space and weight. In Section V, a numerical

TABLE 7 LiBs Module Parameters

Parameters	Symbols	Value
Rated voltage	-	173 V
Rated capacity	-	5.5 Ah
Internal resistance	R_{LiB}	0.096 Ω
Weight	-	0.196 ton
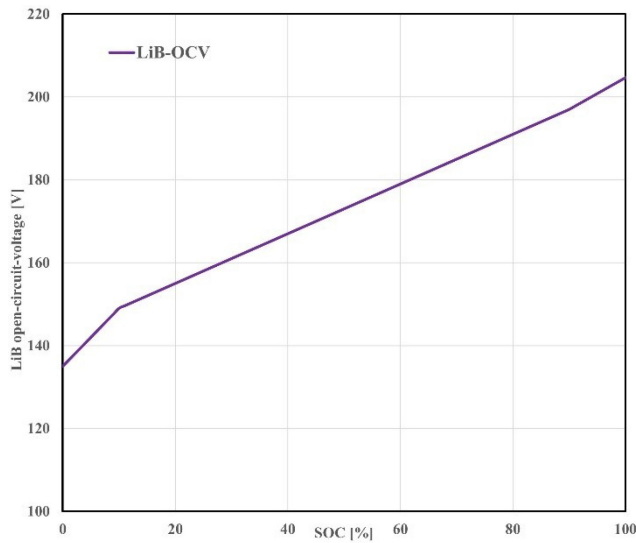
FIGURE 17. OCV characteristics in LiB.

TABLE 8 LiB Capacities and Limits

Pattern	LiB Capacity (SOC 100%)	SOC$_{MIN}$	SOC$_{MAX}$
2Lv.	-	-	-
2S1P	1.903 kWh	20 %	60 %
2S2P	3.806 kWh		
2S3P	5.709 kWh		
2S4P	7.612 kWh		
2S5P	9.515 kWh		

TABLE 9 Car Specification

Parameters	Symbols	Value
Number of trains	-	10
Motor-car trailer-car ratio	-	6M4T
Number of motors	-	24
Motor-car weight (2Lv.)	-	29.8 ton
Trailer-car weight	-	25.0 ton
Wheel diameter	-	0.86 m
Acceleration	-	2.5 km/h/s
Deceleration	-	−3.0 km/h/s
Filter-reactor resistance	R_{FL}	0.1 Ω
DC feeding line voltage	v_f	1500 V

simulation is conducted while considering an actual railway vehicle in order to calculate the amount of energy consumption and regenerative energy with a variable LiB capacity. This facilitates the comparison of the energy-saving effect with that of a normal two-level inverter and the determination of the optimal LiB capacity.

B. CONDITIONS FOR CALCULATION

Table 7 lists the specifications of the LiBs used in the numerical simulation. In this study, the number of series connections of LiBs is maintained at two. This is because the breakdown voltage of the IGBT is assumed to be 3.3 kV, and the surge voltage should not exceed that voltage value. Therefore, the LiBs voltage is basically maintained at 346 V. However, the LiB voltage is considered to change with SOC and the LiB's current in this simulation. Fig. 17 presents LiB OCV characteristics. Furthermore, the LiB output voltage is changed according to the current. Therefore, DCIR corresponds to R_{LiB}, which is 0.096Ω per module. Based on this, the LiB loss is calculated using the LiB current and R_{LiB}.

The optimal LiB capacity is changed according to the number of LiB modules connected in parallel, and in this study, the optimal capacity is examined for one parallel (2S1P) to five parallel (2S5P). The LiB capacity patterns obtained in this study are summarized in Table 8. Based on actual railway

applications, the maximum and minimum SOC of the proposed energy management method are set as 60% and 20%, respectively, for all the capacities [16].

In this simulation, the railway vehicle is driven by an induction motor. The vehicle specifications are listed in Table 9, and it is assumed that four motors are driven by one inverter, and 24 motors are installed in a train set. The weight of the motor car is 29.8 tons, each with the normal two-level inverter traction circuit system, and it is increased in proportion to the number of LiBs in hybrid 3Lv. VSI traction system. However, the weight of the trailer car remains unchanged by the number of LiBs. In addition, 160 passengers weighing 55 kg each are riding in each car.

For the traction circuit system, the overhead line voltage is constant at 1500 V. To calculate the energy consumption, it is necessary to consider the motor loss. Using the motor specifications in Table 10, the copper loss W_c and iron loss W_i are calculated as follows [21]. The iron loss is divided into the hysteresis and eddy current losses.

$$W_c = R_1 \left(i_{1d}^2 + i_{1q}^2 \right) + R_2 \left(\frac{M}{L_2} i_{1q} \right)^2 [\text{W}] \quad (4)$$

$$W_i = k_h f_e B^2 + k_e (f_e B)^2 [\text{kW}]$$
$$= \frac{k_h k_B V_m^2}{f_B} + k_e k_B V_m^2 [\text{kW}] \quad (5)$$

TABLE 10 IM Specifications

Parameters	Symbols	Value
Pole-pairs	P	2
Stator resistance	R_1	0.0971
Rotor resistance	R_2	0.0816
Stator inductance	L_1	0.03012
Rotor inductance	L_2	0.02993
Mutual inductance	M_m	0.02910
Gear ratio	-	6.31
Factor of proportionality	$k_h k_B$	0.0000346
Factor of proportionality	$k_e k_B$	0.000000216

FIGURE 18. Motor torque characteristics in powering.

FIGURE 19. Motor torque characteristics in regeneration.

In equation (4), R_1 is stator resistance, R_2 is rotor resistance, M is mutual inductance, L_2 is rotor inductance. i_{1d} and i_{1q} are the primary-side dq-axis currents of the motor. These currents are calculated using the Runge–Kutta method from the differential equation of the motor. In equation (5), f_e is the inverter frequency, B is the magnetic flux density, V_m is the motor input voltage, and k_h, k_e, and k_B are proportionality constants that are defined.

In the inverter, the switching and conduction losses are generated by the switching devices. In this study, it is considered that IGBT devices with a 3.3-kV breakdown voltage (manufactured by *Hitachi Power Semiconductor Devices*) are used in the normal 2Lv. inverter and hybrid 3Lv. VSI. In particular, the reverse blocking IGBT for hybrid 3Lv. VSI has not been developed, which has a breakdown voltage as high as that of the IGBT used in electric railway vehicles. Therefore, in the numerical simulation of this study, the reverse blocking IGBT is replaced by two IGBTs connected in reverse series. Because the dq-axis motor current is already calculated, the UVW phase current is also calculated. This three-phase current is the collector current in the IGBT module, the forward current in the diode, and the switching loss, conduction loss, and recovery loss are calculated from the data sheet [22].

The loss due to the running resistance is calculated as follows [23].

$$R_{run} = (1.65 + 0.247V)\,m_M + (0.78 + 0.0028V)\,m_T$$
$$+\ 9.81\,\{0.028 + 0.0078\,(n-1)\}\,V^2[\text{N}] \qquad (6)$$

In equation (6), m_M is the load of all the motor cars, m_T is the load of all the trailer cars, n is the number of formations, and V is defined as the train speed.

In the traction system of DC-electrified railways, a filter reactor (FL) is inserted between the inverter and the overhead line, and FL losses are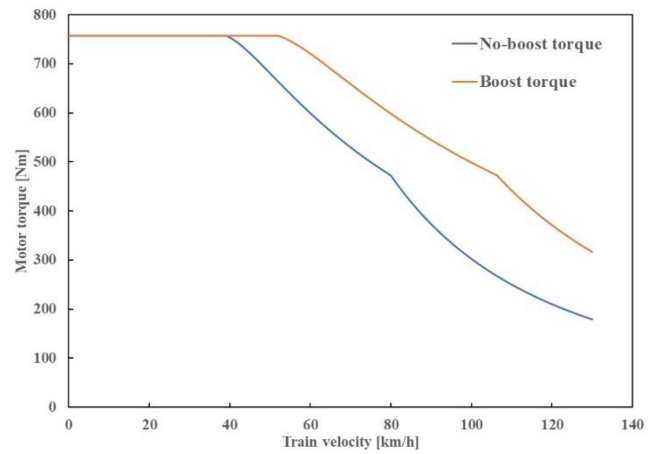 caused by the internal resistance. To calculate the FL loss, it is necessary to calculate the FL current. In this study, the FL current is calculated as follows.
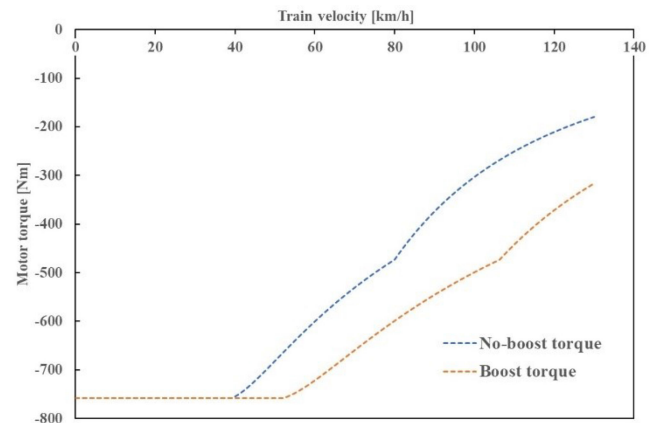
$$i_{FL} = \frac{P_{trc} + W_c + W_i + W_{inv} - P_{LiB}}{v_f}[\text{A}] \qquad (7)$$

In equation (7), P_{trc} is the power of the motor torque [W], and P_{LiB} is defined as the charge/discharge power of the LiBs. i_{FL} from the overhead-line to the inverter can be calculated by dividing P_{LiB} subtracted from the inverter input power by the overhead-line voltage. The FL loss is calculated from i_{FL} and the resistance component of FL, i.e., R_{FL}.

Figs. 18, 19 presents the torque characteristics of the motor during power generation and regeneration. During regeneration, the deceleration is constant, and a mechanical brake is used to compensate for the insufficient braking force of the motor torque. Fig. 20 presents the stations at which the train is assumed to run. There are no gradients or curves between the stations. In addition, the 13 stations are divided into three areas, each with a different maximum speed band. The purpose of this study is to verify the energy-saving effect of various possible speed bands for practical applications. As shown in Table 11, the maximum train speed is changed such that the
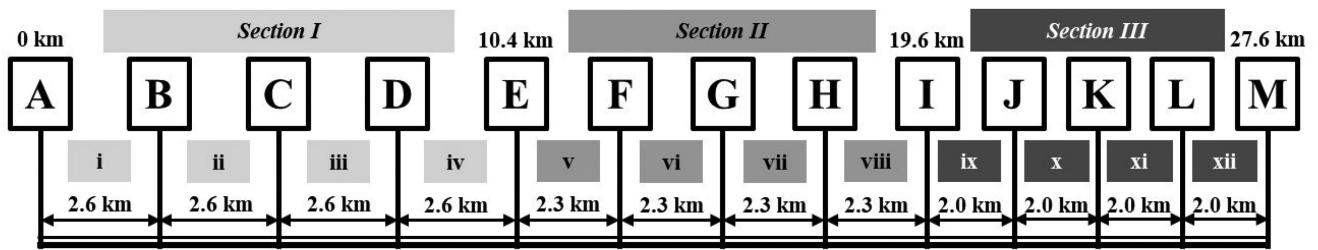
FIGURE 20. Assumed positions of stations.

TABLE 11 Maximum Train Speed

Pattern	*Section I (each distance:2.6 km)*				*Section II (each distance:2.3 km)*				*Section III (each distance:2.0 km)*			
	i	ii	iii	iv	v	vi	vii	viii	ix	x	xi	xii
2Lv.	120.0	120.0	120.0	120.0	100.0	100.0	100.0	100.0	80.0	80.0	80.0	80.0
2S1P	112.4	110.8	110.8	110.8	97.8	97.8	97.8	97.8	79.7	79.7	79.7	79.7
2S2P	110.0	111.0	111.0	111.0	98.0	98.0	98.0	98.0	79.7	79.7	79.7	79.7
2S3P	111.2	111.2	111.2	111.8	98.2	98.2	98.2	98.2	79.7	79.7	79.7	79.7
2S4P	111.6	111.6	111.6	111.4	98.4	98.6	98.6	98.6	79.9	79.9	79.9	79.9
2S5P	112.0	112.0	112.0	112.0	98.8	98.6	98.8	98.8	80.1	80.1	80.1	80.1
											(All units: km/h)	

train runs at the same time as the normal two-level inverter and hybrid 3Lv. VSI, which is different from the motor torque characteristics. The running curve and SOC transition due to the motor running across 13 stations with a two-level inverter and hybrid 3Lv. VSI for each LiB capacity from 2S1P to 2S5P are calculated as the simulation results.

In addition, the energy consumption is evaluated by summing the various losses. The consumption energy and regenerative energy to confirm the energy-saving effect and to optimize the capacity.

C. SIMULATION RESULTS

1) RUN CURVE AND SOC TRANSITIONS

The run curves are presented in Fig. 21. The SOC transitions are presented in Fig. 22. In station Sections I and II, the maximum speed of any capacity of hybrid 3Lv. VSI is lower than that of the two-level inverter, as shown in Table 11. In contrast, station Section III is a relatively low-speed section, and the maximum speed of the hybrid 3Lv. VSI system cannot be much lower than that of the normal inverter systems. This is because the weight of the motor car becomes heavier when the LiB capacity is increased, or the motor torque does not exhibit much of a difference in the relatively low-speed band. As a result, the difference in the run curves between the normal two-level inverter and hybrid 3Lv. VSI is more significant when the maximum speed band of the vehicle is higher.

The SOC transition graph presented in Fig. 22 is discussed below. It is confirmed that the transitions between the boost and non-boost modes are properly performed without exceeding SOC_{MAX} or falling below SOC_{MIN} in any LiB capacity. Especially in the case of 2S1P, it is easy to reach SOC_{MAX}
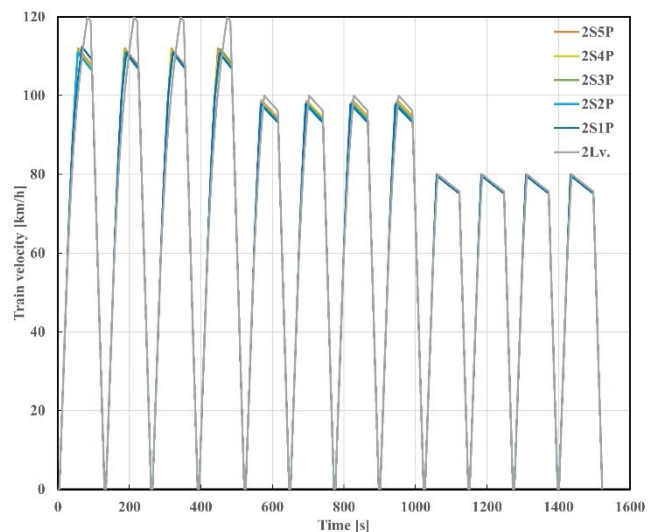

FIGURE 21. Run curve.

and SOC_{MIN} during powering and regeneration. However, in the case of 2S2P and greater capacities, the limits of SOC are not reached in just one run, but they are reached in multiple runs.

2) NUMBER OF BATTERIES AND ENERGY-SAVING EFFECT

Table 12 lists the values of loss and regenerative energy. Using these values, the graphs of the energy consumption and regenerative energy are presented in Figs. 23–24. In addition, Table 13 presents the ratio of the regenerative energy to the total input energy, which is the sum of the energy consumption

TABLE 12 Consumption-Energy Breakdown& Regenerative Energy

Pattern	Energy loss [kWh]							Regenerative energy [kWh]
	Copper loss	Iron loss	Running resistance loss	Mechanical brake loss	FL loss	LiB loss	Inverter loss	
2Lv.	26.87	4.48	64.38	175.24	18.83	-	7.84	272.05
2S1P	21.75	4.84	63.74	95.82	18.53	19.19	20.12	305.21
2S2P	21.79	4.84	63.92	97.99	18.70	10.73	18.81	305.01
2S3P	21.99	4.87	64.16	101.51	18.59	7.27	16.32	306.46
2S4P	22.11	4.89	64.39	104.67	18.62	5.60	15.08	307.36
2S5P	22.24	4.93	64.64	108.36	18.86	4.62	14.39	308.85
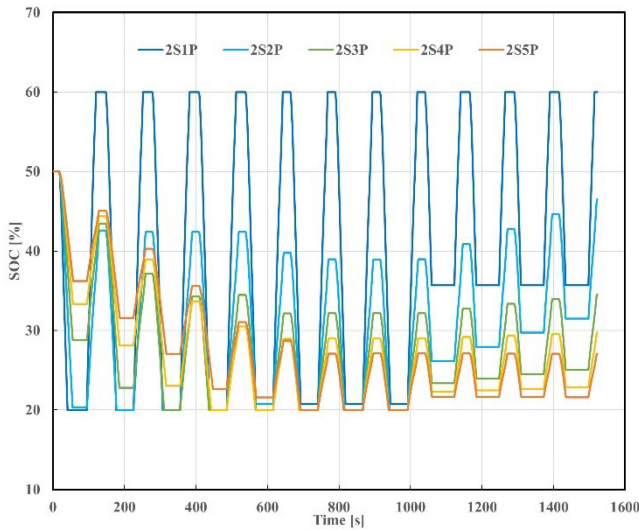
FIGURE 22. SOC transitions.

FIGURE 24. Regenerative energy.

TABLE 13 Rate of Regenerative Energy

Pattern	Energy consumption [kWh]	Regenerative energy [kWh]	Rate of regenerative energy [%]
2Lv.	289.80	272.05	47.75
2S1P	223.87	305.21	55.57
2S2P	217.97	305.01	56.30
2S3P	218.39	306.46	56.63
2S4P	220.28	307.36	56.63
2S5P	223.64	308.85	56.48

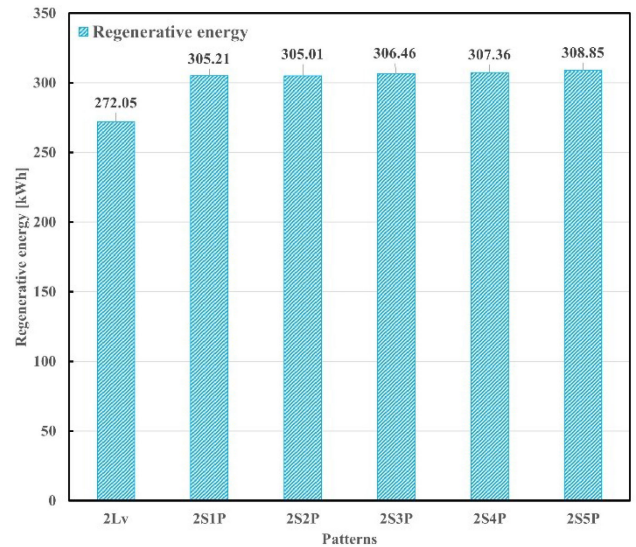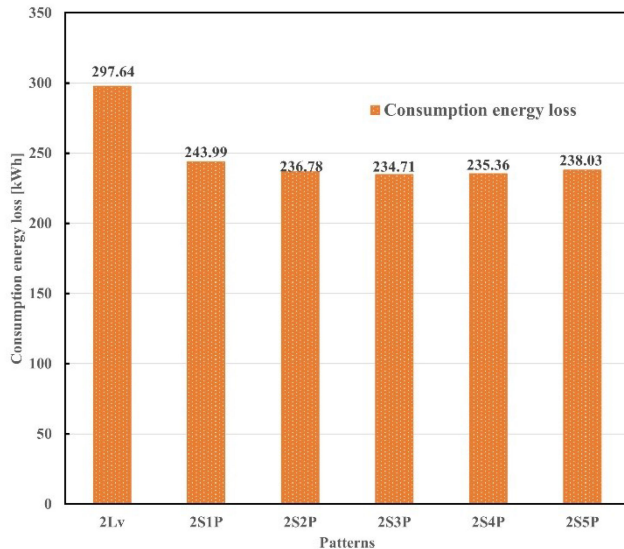**FIGURE 23.** Consumption energy loss.

and regenerative energy. From Fig. 23, driven by the hybrid 3Lv. VSI with proposed energy management method reduces the energy consumption by approximately 18–21% compared to the case of the normal two-level inverter. In particular, it is

also confirmed that the energy consumption of 2S3P is the lowest, and it is reduced by approximately 21.1% as compared to that of the normal inverter. On comparing 2S1P and 2S2P, 2S3P, the energy-consumption reduction effect of 2S3P is found to be greater than that of 2S1P and 2S2P because the time for which it is operated in boost mode is longer. However, the reduction effect for capacities above 2S4P is smaller than that for 2S3P. On observing Table 12, it is confirmed that there is an increasing trend of the various losses, except for the LiB loss. This is caused by the decrease in the acceleration performance because of the increase in the train

weight, which occurs for a longer time during powering. The LiB loss decreases as the LiB capacity increases because the value of the internal resistance is decreased on increasing the number of parallel connections. Next, the regeneration energy presented in Fig. 24 is discussed. In any case of LiB capacities, the regenerative energy is greater than that of the normal two-level inverter system. This is because the advantage of a mechanical brake is reduced by improving the motor torque characteristics. The regenerative energy value is thus different for each capacity because the speed at the start of regeneration is different.

3) OPTIMAL BATTERY CAPACITY IN THE FLAT LINE SECTION

The results of energy consumption and regenerative energy have been discussed above, and the ratio of the regenerative energy is used to optimize the LiB capacity. This value indicates how much energy is returned as regenerative energy from the total input energy to the railway vehicle. Therefore, this value indicates the energy-saving effect determined by the increase or decrease in the energy consumption and regenerative energy. The results in Table 13 show that 2S3P and 2S4P has the highest regeneration rate. Because 2S3P can achieve the same energy saving effect as 2S4P with less capacity, the LiB capacity at 2S3P provides the greatest energy-saving effect when the train runs at various speeds in the flat line section.

VI. CONCLUSION

In this paper, a hybrid-voltage three-level inverter that contributes to the further energy savings of DC-electrified railway vehicles is focused on, and the PWM operation features and LiB power-flow control realized using a modulation wave offset are explained. Based on these features, an energy-management method for realizing energy savings is proposed in Section III. In the proposed method, the power flow control of the batteries with the modulation wave offset and pulse mode are determined by the inverter frequency and SOC of the LiBs for both powering and regeneration.

In Section IV, the operation and effectiveness of the proposed method are verified via mini-model experiments. Specifically, the pulse mode of the inverter and the offset are selected correctly according to the SOC and inverter frequency. Furthermore, we also confirm that the charging/discharging power flow of the LiBs is controlled by the selected pulse mode and offset. From the experimental results, the proposed energy-management method is verified to operate as engineered.

In Section V, numerical simulations are used with the consideration of an actual railway vehicle to verify the extent of the energy-saving effect realized as compared to that of a normal two-level inverter when the hybrid 3Lv. VSI is operated using the proposed management method. In addition, the LiB capacity is focused on in the hybrid 3Lv. VSI and optimized to maximize the energy-saving effect. These examinations are performed by calculating the energy consumption

and regenerative energy using the loss model. Based on the results of the numerical simulation, the energy consumption is reduced by approximately 18–21% on using the hybrid 3Lv. VSI system with the proposed energy management method. This energy saving effect is mainly obtained by applying the hybrid DC power source configuration. As an energy-saving effect per LiB capacity, two LiBs connected in series and three in parallel provide the optimal capacity based on the value of the regeneration rate.

REFERENCES

[1] Y. Taguchi, M. Ogasa, H. Hata, H. Iijima, A. Ohtsuyama, and T. Funaki, "Simulation results of novel energy storage equipment series-connected to the traction inverter," in *Proc. Eur. Conf. Power Electron. Appl.*, 2007, pp. 1–9.

[2] M. Shimada, Y. Miyaji, T. Kaneko, and K. Suzuki, "Energy-saving technology for railway traction systems using onboard storage batteries," *Hitachi Rev.*, vol. 61, no. 7, pp. 312–318, 2012.

[3] H. Kobayashi and K. Kondo, "Control method for increasing motor power of DC-electrified railway vehicles with an onboard energy storage system," *IEEJ J. Ind. Appl.*, vol. 10, no. 5, pp. 520–527, 2021.

[4] H. Kobayashi and K. Kondo, "A novel control method of parallel connected onboard energy storage system for DC-electrified rail vehicle to increase traction motor power," in *Proc. Int. Symp. Power Electron., Elect. Drives, Automat. Motion*, 2020, pp. 612–617.

[5] H. Fujita, "Emerging technologies for multilevel converters in Japan," *IEEJ J. Ind. Appl.*, vol. 1, no. 2, pp. 95–101, 2012.

[6] L. Ben-Brahim, A. Gastli, T. Yoshino, T. Yokoyama, and A. Kawamura, "Review of medium voltage high power electric drives," *IEEJ J. Ind. Appl.*, vol. 8, no. 1, pp. 1–11, 2018.

[7] R. Chattopadhyay *et al.*, "Low-Voltage PV power integration into medium voltage grid using high-voltage SiC devices," *IEEJ J. Ind. Appl.*, vol. 4, no. 6, pp. 767–775, 2015.

[8] K. Kondo, "Basic study on an EDLC and DC voltage hybrid traction system with a direct converter," in *Proc. Int. Power Electron. Conf.*, 2010, pp. 2147–2152.

[9] Y. Ide, A. Shimada, and K. Kondo, "Study on the PWM methods of the unbalanced input voltage three level inverter with the energy storage device," in Proceedings 14th european conference on power electronics and applications, 2011, pp. 1–9.

[10] K. Yoshimoto, K. Maikawa, and S. Satou, "Novel multiple DC-inputs direct electric power converter," *EPE J.*, vol. 20, pp. 36–41, 2010.

[11] K. Yoshimoto, "Multiple-DC-inputs direct power converter D-EPC using multiple input leg reduction topology and its control," *IEEJ J. Ind. Appl.*, vol. 9, no. 3, pp. 298–304, 2020.

[12] S. M. Lukic, J. Cao, R. C. Bansal, F. Rodriguez, and A. Emadi, "Energy storage systems for automotive applications," *IEEE Trans. Ind. Electron.*, vol. 55, no. 6, pp. 2258–2267, Jun. 2008.

[13] K. Fujii, T. Kikuchi, H. Koubayashi, and K. Yoda, "1-MW advanced T-type NPC converters for solar power generation system," in *Proc. 15th Eur. Conf. Power Electron. Appl. (EPE)*, 2013, pp. 1–10.

[14] K. Komatsu *et al.*, "New IGBT modules for advanced neutral-point-clamped 3-level power converters," in *Proc. Int. Power Electron. Conf. - ECCE ASIA*, 2010, pp. 523–527.

[15] Y. Ide, A. Shimada, and K. Kondo, "Study on the PWM methods of the unbalanced input voltage three level inverter with the energy storage device," in *Proc. 14th Eur. Conf. Power Electron. Appl.*, 2011, pp. 1–9.

[16] N. Shiraki, H. Satou, and S. Arai, "A hybrid system for diesel railcar series ki-ha E200," in *Proc. Int. Power Electron. Conf. - ECCE ASIA*, 2010, pp. 2853–2858.

[17] T. Mizobuchi, K. Kondo, Y. Dairaku, T. Shinomiya, and K. Ishikawa, "Energy management of battery on hybrid voltage source three level inverter for energy saving railway vehicles," in *Proc. 23rd Int. Conf. Elect. Machines Syst.*, 2020, pp. 1089–1094.

[18] Y. Song, M. Park, M. Seo, and S. W. Kim, "Improved SOC estimation of lithium-ion batteries with novel SOC-OCV curve estimation method using equivalent circuit model," in *Proc. 4th Int. Conf. Smart Sustain. Technol. (SpliTech)*, 2019, pp. 1–6.

[19] H. Miyamoto, M. Morimoto, and K. Morita, "On-line SOC estimation of battery for wireless tram car," in *Proc. 7th Int. Conf. Power Electron. Drive Syst.*, 2007, pp. 1624–1627.

[20] L. Gao, S. Liu, and R. A. Dougal, "Dynamic lithium-ion battery model for system simulation," *IEEE Trans. Compon. Packag. Technol.*, vol. 25, no. 3, pp. 495–505, Sep. 2002.

[21] R. Ikeda, S. Yusya, and K. Kondo, "Study on design method for increasing power density of induction motors for electric railway vehicle traction," in *Proc. IEEE Int. Electric Machines Drives Conf.*, 2019, pp. 1545–1550.

[22] Hitachi Power Semiconductor Device, Ltd., "IGBT 3300V F-Version 1in1 IGBT." MBN1200F33F datasheet, Oct. 2017.

[23] S. Manabe, T. Ogawa, Y. Imamura, S. Minobe, J. Kawamura, and M. Kageyama, "A method of calculating running resistance using monitoring devices for energy simulators," in *Proc. Int. Conf. Elect. Syst. Aircr., Railway, Ship Propulsion Road Veh.*, 2015, pp. 1–6.

TADASHI MIZOBUCHI was born in Tokushima, Japan, in 1997. He received the B.E. degree from the School of Advanced Science and Engineering, Waseda University, Tokyo, Japan, in 2020.

Since April 2020, he has been a student with the Department of Electrical Engineering and Bioscience, Graduate School of Advanced Science and Engineering, Waseda University.

His research interests include power electronics, hybrid systems, and AC motor drives. He is a Student Member of the Institute of Electrical Engineers of Japan (IEEJ).

KEIICHIRO KONDO (Member, IEEE) received the B.S. and Ph.D. degrees in engineering from the Department of Electrical Engineering, School of Science Engineering, Waseda University, Tokyo, Japan, in 1991 and 2000, respectively.

He joined the Railway Technical Research Institute, Kokubunji, Japan, in 1991 and was engaged in the research and development for power electronics applied to railway vehicle traction. From April 2007 to March 2018, he was with the Electrical and Electric Engineering Course, Graduate School and Faculty of Engineering, Chiba University, Chiba, Japan. Since April 2018, he has been a Professor with the Faculty of Science Engineering, Waseda University. His current research interests include power electronics, AC motor drives, energy storage devices, and wireless power transmission and their applications to railway systems.

Prof. Kondo titled Professional Engineer Japan (Mechanical Engineering, Technical Management). He is a Senior Member of the Institute of Electrical Engineers of Japan (IEEJ).

YOSUKE DAIRAKU was born in Ibaraki, Japan, in 1996. He received the B.E. and M.E. degrees from the Graduate School of Science and Engineering, Chiba University, Chiba, Japan, in 2018 and 2020, respectively.

In 2020, he joined Mito Works, Hitachi Ltd. He is engaged in the development of electrical components for rolling stock including power electronics, hybrid systems, and battery applications.

He is a Member of the Institute of Electrical Engineers of Japan (IEEJ).

TAKESHI SHINOMIYA was born in Shizuoka, Japan, in 1981. He received the B.S. degree from the School of Faculty of Engineering, Shibaura Institute of Technology, Tokyo, Japan, in 2005.

In 2005, he joined Mito Works, Hitachi, Ltd. He is engaged in the development of electrical components for rolling stock including power electronics, hybrid systems, and AC motor drives.

He is a Member of the Institute of Electrical Engineers of Japan (IEEJ).

KATSUMI ISHIKAWA received the B.S. degree from Ibaraki University, Ibaraki, Japan, in 1991, and the M.S. degree from Tsukuba University, Ibaraki, Japan, in 1993, and the Dr. Eng. degree from Hokkaido University, Hokkaido, Japan, in 2014.

He joined the Hitachi Research Laboratory, Hitachi, Ltd., Ibaraki, Japan, in 1993 and was engaged in applied research into power semiconductors with Hitachi Research Laboratory, Advanced Research Laboratory, and Hitachi Power Semiconductor Device, Ltd. In 2013, he moved Mito Works, Hitachi, Ltd., to coordinate the development of electrical components for rolling stock. Since 2019, he has been engaged in coordinating areas, such as new investment and global research and development for the rolling stock and electrical components businesses with COO Rolling Stock (Japan) Office, Railway Systems Business Unit, Hitachi, Ltd.

He is a Senior Member of the Institute of Electrical Engineers of Japan (IEEJ) and a Member of Japan Railway Engineer's Association (JREA).